Synthesis of Fe-Salen-MCM-41 Hybrid Catalysts

Syuhada Mohd Tahir
Halimaton Hamdan
Syahidah Mohd Tahir
Mariya Mohd Tahir

ABSTRACT

MCM-41 with SiO_2/Al_2O_3 ratios =60 were used as a support for heterogenization of Fe (III) salen complex to form hybrid catalysts. Flexible ligand method was applied for immobilization of complex onto the supports. The physical properties of these hybrid catalysts were characterized using XRD, FTIR, UV-Vis DR, EDX and BET. The powder XRD data confirmed that the structural order of MCM-41 remained intact after the encapsulation process. FTIR and EDX studies show the presence of Fe (III) in the hybrid catalyst sample. UV-Vis DR analysis reveals that the free and encapsulated complexes exhibit the tetrahedral geometry. BET results show that the pore volumes of the synthesized hybrid catalysts are lower than the neat MCM-41, thus proved successful encapsulation.

Keywords: MCM-41, hybrid catalyst, Salen complex

Introduction

The past decade has seen great advances in the synthesis of new periodical porous materials. These are due to the importance of porous materials as catalysts in many industrial applications. Their large surface areas enhance the catalytic and sorptive activity. Two main types of porous materials, according to their pore size, are mesoporous and microporous materials. Amorphous mesoporous materials represent an important class of porous inorganic solids, with limited long-range order and usually have a wide distribution of pore sizes. In contrast, microporous molecular sieves have a crystalline structure with a very narrow pore size distribution. It is generally presumed that a mesoporous material with uniform pores would have wide utility in catalysis. Therefore, considerable effort had been devoted to synthesize frameworks with pore diameters within the mesoporous range (Ravikovitch et al. 1997).

The MCM-41 materials possess a regular array of hexagonal, uniform and unidimensional mesopores. The high surface area, moderate acidity and distinct adsorption properties of MCM-41, open up new potential applications as catalysts and catalyst supports. Like in zeolites, the framework of MCM-41 is based on an extensive three-dimensional network of oxygen ions that occupied tetrahedral cation sites, and in addition to the Si^{4+}, other cations can also occupy these sites. MCM-41 exhibits pore system with wide range adjustable sizes that expands the range on zeolitic micropores. The development of strategies for the synthesis of materials with controllable pore sizes within as wide ranges as possible has been targeted by many research groups lately (Daud, 2006).

Recently, preparation of organic-inorganic hybrid catalysts based on porous materials are gaining great interest particularly for the synthesis of fine chemicals in the liquid phase at lower temperatures. The heterogeneous catalysis is obviously advantageous in the catalyst recovery and eco-benignity. Most of industries today are still using homogeneous catalyst, which is the main factor of environmental pollution because of the uses of solvents. Thus, the heterogenization of homogeneous catalysts has emerged as a focus of nowadays research (Doménéch et al. 2000). One elegant way involves the immobilization of active catalytic site onto a solid having a large surface area such as zeolites and mesoporous materials to form the hybrid catalyst. Hybrid catalysts prepared by immobilization of catalytically active organometallic complexes on certain supports produce both high activity and selectivity of homogeneous catalysts and easy separation of reaction products by heterogeneous catalyst. These hybrid catalysts can be synthesized by a number of methods such as adsorption of the organic species into the pores of the support, construction of the organic molecule piece by piece within the confined space of cavities of the support, attachment of the desired

functionality to the support by covalent bond formation and direct synthesis into the final composite material (Wight and Davis 2002).

A crucial part to be considered in heterogenizing a homogenous catalyst is the pore size of the support. Several researches have been carried out on pore size modification in order to get desired pore size. Hu et al. (2000) has successfully immobilized AlCl$_3$ on MCM-41 mesoporous silica of different pore sizes to form a novel shape-selective catalyst for Friedel-Crafts alkylation of benzene with long chain olefins. The result of the study showed that the selectivity toward the monoalkylated product is strongly influenced by the pore size of the carrier material. This demonstrates the opportunities offered by the micelle-templating method to tailor shape-selective catalysts for reactions with bigger molecules (Hu et al. 2000). Sayari (1996) pointed out the importance of pore size flexibility of mesoporous molecular sieves in various areas; acid catalysis, redox catalysis and other miscellaneous applications. Kubota at al. (2006) and his co-workers had studied the role of surfactant as structure-directing agent to obtain desired pore size in synthesizing organic-inorganic hybrid catalyst extensively. They found that the organic-functionalized molecular sieves are most effective when the supports have large pore volume and surface area.

Thus, the objectives of this study are; i) To synthesize MCM-41 with different pore size, using various carbon chain length alkyltrimethylammonium bromide surfactants, and ii)   To synthesize Fe-Salen-MCM-41 hybrid catalyst by incorporating Fe-Salen complex into the modified pore of mesoporous host via flexible ligand method.

Experimental

The methodology for this research is given in the following Figure 1.
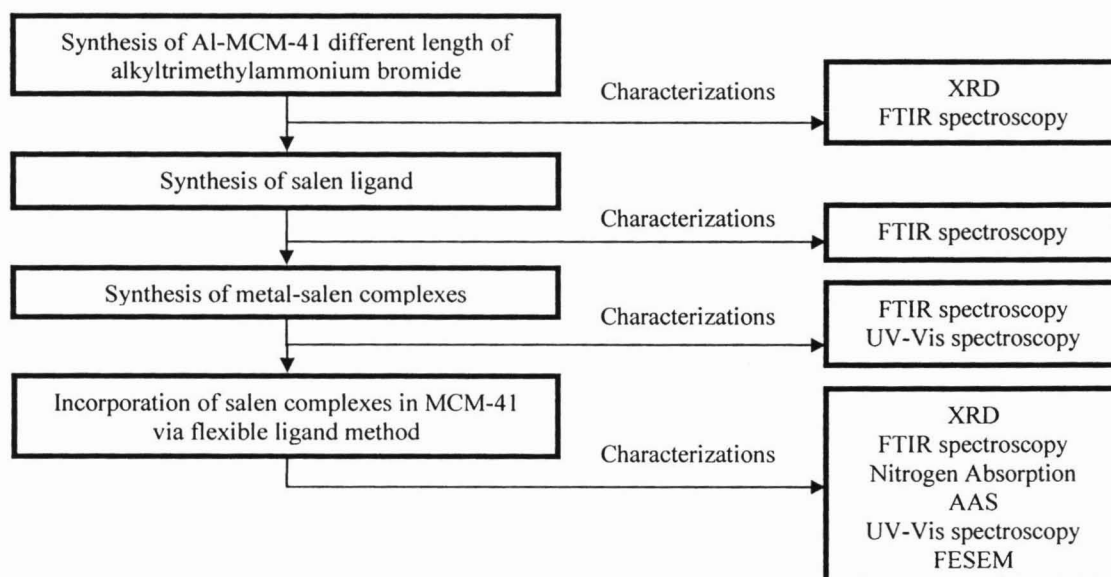
Figure 1: Flowchart of research methodology

The synthesis of Al-MCM-41, with SiO$_2$/Al$_2$O$_3$ ratios = 60, was carried out according to the molar composition:

6SiO$_2$: xNaAlO$_2$: CTMABr : 1.5Na$_2$O : 0.15(NH$_4$)$_2$O : 250H$_2$O

The sodium silicate solution was prepared by mixing 7.7 g of rice husk ash with 100.0 g of doubly distillated water and 2.5 g of sodium hydroxide. The solution was stirred at 80°C for 2 h. In another

propylene bottle, cetyltrimethylammonium bromide, $C_{16}H_{33}(CH_3)_3NBr$ and 0.4 g of sodium aluminate, $NaAlO_2$ were dissolved in 100.0 g of distilled water and 0.2 g of ammonium hydroxide, NH_4OH. The mixture was also heated and stirred at 80°C for 1 h. After that, the sodium silicate solution, Na_2SiO_3 was added drop wise into the propylene bottle containing the template solution and was simultaneously stirred at 97°C. The resulting mixture was then aged overnight at ~97°C in oven. After cooling it to an ambient temperature, the pH of the gel was adjusted to ~10.2 by addition of acetic acid, CH_3COOH (30 wt%). The

subsequent 24 h ageing and pH adjustment procedures were repeated two times. The precipitate was then filtered, washed with distilled water, dried in oven at 97°C and finally calcined at 550°C to remove the organic template. The calcination temperature was increased from room temperature to 550°C for 6 h and maintained at that temperature for another 10 h. The preparation procedure was repeated using the other two chain length of templates, which are decyltrimethylammonium bromide, $C_{10}H_{21}(CH_3)_3NBr$ and octadecyltrimethylammonium bromide, $C_{18}H_{37}(CH_3)_3NBr$.

The salen (N,N'-bis(salicylaldehyde)ethylene diamine) ligand was prepared by dissolving 0.6 g (0.01 mole) ethylene diamine (en), and 2.4 g (0.02 mole) salicylaldehyde in 25 mL and 100 mL absolute ethanol (99.7 %v/v) respectively. The resulting salicylaldehyde solution was then added dropwise into the previously prepared ethylene diamine solution. The mixture was refluxed at 80°C for 1 h followed by cooling it on ice. The resulting yellow plate crystal was then filtered and washed with petroleum ether. In order to prepare the complex, 2.7 g (0.01 mole) of the prepared salen ligand was reacted with 1.6 g (0.01 mole) of ferric trichloride, $FeCl_3$ in 50 mL refluxing ethanolic solution for 2 hours at 100°C. The resulting precipitate was then filtered while it was still hot and washed with distilled water. The complexes were obtained by drying the sample overnight at 100°C.

The flexible ligand procedure was started by refluxing 2.0 g of Al-MCM-41 sample in 150 mL of 0.002 M ferum ion solutions at 80°C for 6 h. The resulting solid was recovered by filtering, washing with deionized water and drying in oven at 110°C. The final product was calcined at 500°C for 5 h to remove the organic moieties. The ferum-salen-MCM-41 catalysts were finally obtained by refluxing 0.3 mmole of salen ligand and the prepared ferum-MCM-41 in ethanolic solution at 80°C for 6 h under flowing nitrogen. The catalysts were collected by filtering, washing and drying. The excess of metal ions in the solid were removed by ion exchange, where the catalyst was mixed with 0.01 M NaCl solution, stirred and washed with hot water. The soxhlet extraction process was carried out in order to remove the unreacted ligand. Figure 2 shows the complete heterogenization process.
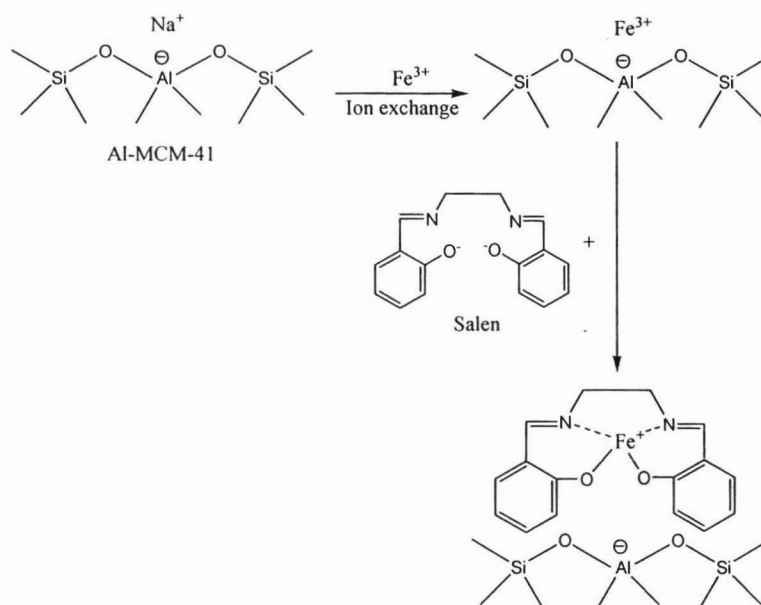

Figure 2: Preparation of hybrid catalysts via flexible ligand method

Results and Discussion

Synthesis of Al-MCM-41

X-ray diffractograms of Al-MCM-41(C_{16}) and Al-MCM-41(C_{18}) samples show a high intensity diffraction peak around 2.5° and two other low intensity peaks at higher 2θ values while Al-MCM-41(C_{10}) sample show the absence of (110) and (200) planes because of the high amorphous phase or deformation of planes. The diffraction peaks positions show that the lattice geometry of MCM-41 is hexagonal (Lau, 2005). Figure 3 shows the X-ray diffractogram of Al-MCM-41(C_{10}), Al-MCM-41(C_{16}) and Al-MCM-41(C_{18}), of both, as-synthesized and calcined samples. The presence of (100) diffraction peak indicates the hexagonal lattice structure of the synthesized sample (Daud, 2006). The crystallinity of the as-synthesized sample increases upon calcination, which is evident by the increase in the intensity of those peaks. Besides that, the calcination also results in shifting of 2θ angle of as-synthesized sample towards a higher value. This is due to the shrinkage effect as a result of template removal, which further decreases the pore diameter of sample (Karandikar et al. 2004). The repeating distance between two pore centers, a_o can be calculated by $a_o = (2/\sqrt{3})$ d_{100} and the resulting value can be used to determine the pore diameter by subtracting 1.0 nm as an approximate value for the pore wall thickness (Daud, 2006; Grun et al. 1999). Table 1 shows the data interpretation of X-ray diffractogram of the three Al-MCM-41 samples. The data clearly shows the increasing trend in the pore diameter of the samples as the length of the templates used was increased.
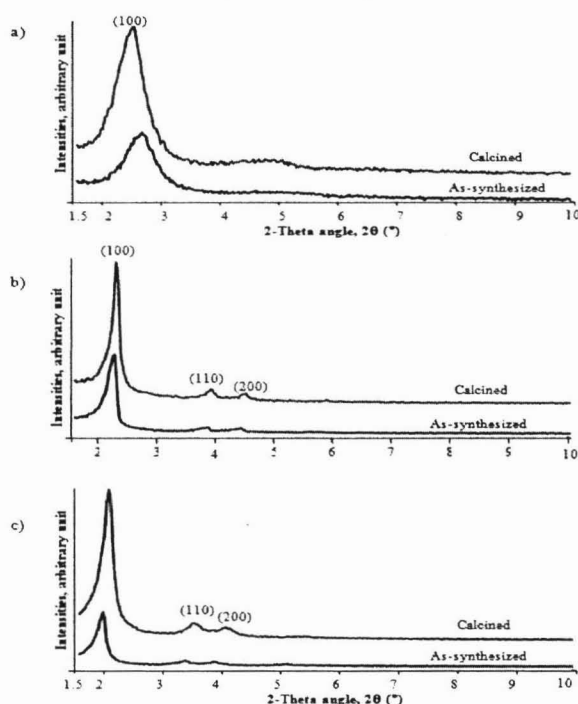

Figure 3: X-ray diffractograms of; a) Al-MCM-41(C_{10}), b) Al-MCM-41(C_{16}), c) Al-MCM-41(C_{18})

Generally, the FTIR spectra of all the three Al-MCM-41 samples show six main absorption peaks at 3400, 1200, 1000, 960, 800 and 450 cm^{-1}. Figure 4 shows the FTIR spectrum for Al-MCM-41(C_{10}), Al-MCM-41(C_{16}) and Al-MCM-41(C_{18}), of both, as-synthesized and calcined samples. As listed in Table 1, the presence of internal asymmetric stretching is indicated by peaks in the range of 1200-900 cm^{-1}. Both as-synthesized and calcined samples, show strong vibration peaks at 1200 and 1000 cm^{-1}, due to asymmetric stretching of TO_4 framework (Daud, 2006), which T is representative for Al or Si. The presence of Si-OH

terminal stretching and symmetric stretching of TO_4 can be observed at the 900 and 800 cm^{-1}, respectively, while the peaks for T-O bending mode appear at approximately 450 cm^{-1} (Flanigen, 1976). The as-

synthesized samples show two more absorption peaks at 2900-2800 and 1400 cm^{-1}, which show the presence of C-H and C-N bond stretching, respectively, which are due to the presence of template in the samples. The spectra of samples after calcination show the absence of these two peaks indicates that the removal of all templates was successful (Hamdan et al. 2005). The O-H stretching peak of the calcined samples is broader than the as-synthesized ones because of the fact that calcination results in more silanol groups and provides vacant spaces to occupy more water molecules adsorbed on the surface of support via formation of hydrogen bonding with those Si-OH groups (Daud, 2006; Hamdan et al. 2005; Rino, 2003).
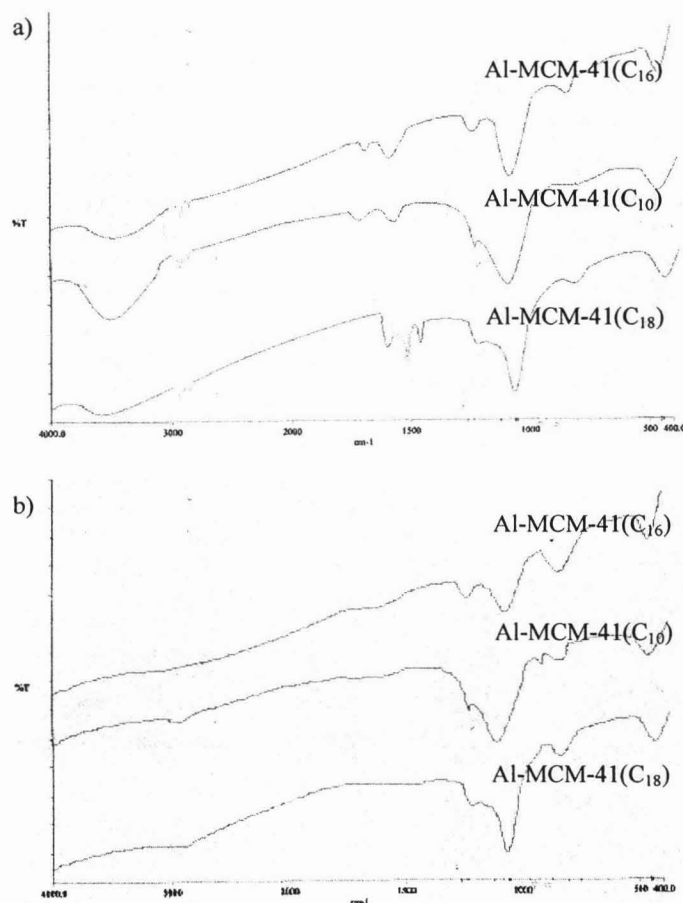
Figure 4: FTIR spectra of Al-MCM-41(C$_{10}$), Al-MCM-41(C$_{16}$) and Al-MCM-41(C$_{18}$) samples; (a) As synthesized and (b) Calcined

Table 1: Vibrational mode of Al-MCM-41(C$_{10}$), Al-MCM-41(C$_{16}$) and Al-MCM-41(C$_{18}$) samples before and after calcination

| Samples	As-synthesized			Calcined		
	C$_{10}$	C$_{16}$	C$_{18}$	C$_{10}$	C$_{16}$	C$_{18}$
C-H stretching (cm^{-1})	2924, 2892	2950, 2920	2920, 2845	-	-	-
TO$_4$ stretching (cm^{-1}) Asymmetric	1227, 1070	1225, 1070	1227, 1072	1232, 1097	1235, 1098	1237, 1089
Symmetric	796	816	775	813	837	849
C-N stretching (cm^{-1})	1363	1465	1460	-	-	-
Si-OH terminal (cm^{-1})	989	902	981	991	965	989
T-O bending (cm^{-1})	458	459	458	453	458	461

The surface area and pore volume analyses were in good agreement with data collected from XRD analyses. As shown in Table 2, the surface area increases proportionally with the increase of surfactant length.

Table 2: Specific surface area (BET) and pore volume data of Al-MCM-41 samples

Sample	Specific surface area, BET (m^2/g)	Pore volume (cm^3/g)
Al-MCM-41(C_{10})	665	0.71
Al-MCM-41(C_{16})	904	0.97
Al-MCM-41(C_{18})	1017	1.09

Synthesis of Salen Ligand

Generally, about $93 \pm 5\%$ yield of yellow shiny plates of salen was obtained and the melting point of the ligand is 125.3°C. Figure 5 shows the FTIR spectrum of synthesized bright yellow salen ligand. This ligand shows seven main absorption peaks around 3500, 3100-2900, 1600, 1570-1490, 1450-1410, 1300-900 and 800-600 cm^{-1}, which show the presence of O-H stretching, C-H sp^2 and C-H sp^3 stretching, C=N stretching, C=C aromatic stretching, CH_2 bending, C-N and C-O stretching and C-H aromatic bending, respectively. Table 3 below lists the bond vibrational frequency of the prepared salen ligand (Daud, 2006).
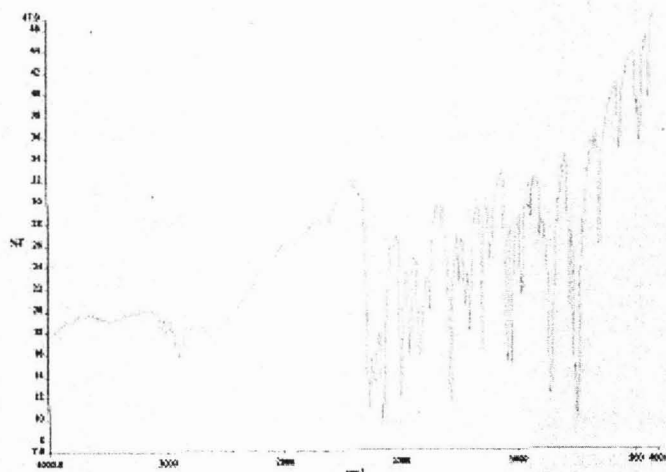
Figure 5: FTIR spectrum of synthesized salen ligand

Table 3: Vibrational modes of the synthesized salen ligand

Characteristic vibration	Wavenumber, $1/\lambda$ (cm^{-1})
O-H stretching	3501
C-H sp^2 stretching	3095
C-H sp^3 stretching	2900
C=N stretching	1635
C=C aromatic stretching	1577 and 1497
CH_2 bending	1460
C-N and C-O stretching	1371-980
C-H aromatic bending	857-647

Synthesis of Fe (salen) Complex

The FTIR spectrum of Fe (salen) complex is shown in Figure 6. Like salen ligand molecule, the main absorption peaks of metal-salen complex were observed in two different areas; 3000 cm^{-1}-2800 cm^{-1} and

$1600cm^{-1}$-400 cm^{-1}. The formation of metal-ligand interaction results in shifting of the C=N absorption peak to a lower wavenumber due to the decrease in electron density as a result of covalent coordinate bond formation (Daud, 2006; Kim & Park, 2000). The C=N bond now shows a single bond characteristic and absorb infrared light at much lower frequency (Daud, 2006). Table 4 lists the vibrational frequencies of synthesized ligand and complex.
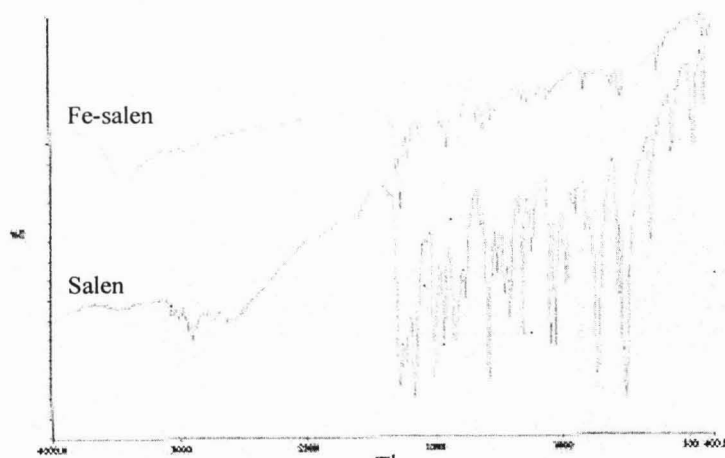

Figure 6: FTIR spectra of salen ligand and Fe (salen) complex

Table 4: Vibrational modes of salen and Fe (salen) complex

Characteristic vibration	Wavenumber, $1/\lambda$ (cm^{-1})	
	Salen	Fe(salen)
C-H sp^2 stretching	3095	3025
C-H sp^3 stretching	2900	2915
C=N stretching	1635	1629
C=C aromatic stretching	1577 and 1497	1545 and 1445
CH$_2$ bending	1460	1384
C-N and C-O stretching	1371-980	1305-905
C-H aromatic bending	877-647	757-618

Figure 7 shows the UV-Vis spectra of Fe (salen) complex. The complex gives a broad absorption at 455 nm assigned to the charge transfer transition between the metal and ligand (d-π^*) in the –C=N-M group. The presence of this charge transfer band is due to the excitation of electron from a predominantly metal centered orbital to a predominantly ligand centered orbital. Another broad adsorption band observed at 538 nm is due to d-d electronic transition (Daud, 2006; Balkus & Gabrielov, 1995). This d-d transition occurs in the visible region of the spectra, thus contributes to the bright colour of complex. The interaction, which occurs as ligand, is near to the metal ion center results in splitting of the metal d orbital (Daud, 2006). Since the d-d transition is not allowed, the intensity of this peak is very low (Rino, 2003; Shriver, 1999).
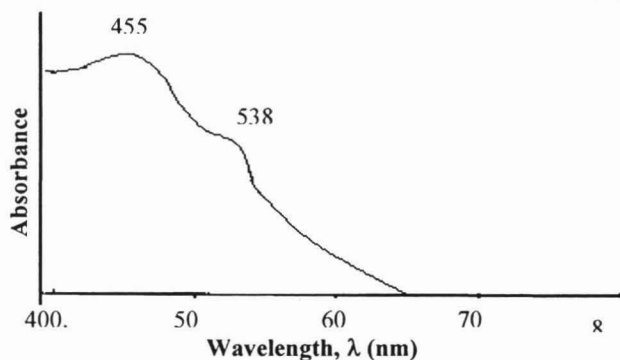
Figure 7: UV-Vis spectra of the Fe(salen) complex

Heterogenization of homogenous catalyst via flexible ligand method

As shown in Figure 8 below, in general, all catalyst samples obtained from heterogenization process show similar FTIR, which proved that the hexagonal Al-MCM-41 framework remained unchanged after the immobilization process. The presence of absorption peaks at 1643 cm^{-1}, 1605 cm^{-1} to 1546 cm^{-1}, 1451 cm^{-1} and 1340 cm^{-1} represent the vibrations of C=N stretching, C=C stretching, CH$_2$ bending and C-O stretching respectively.

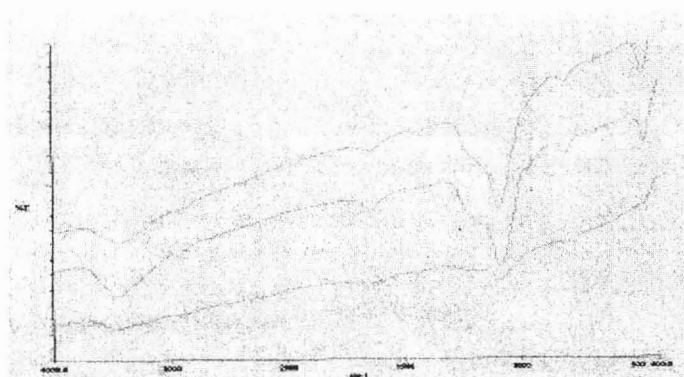Figure 8: FTIR spectra of a) Fe-salen-MCM-41(C$_{10}$), b) Fe-salen-MCM-41(C$_{16}$) and c) Fe-salen-MCM-41(C$_{18}$)

Table 5 lists the surface properties data of the three hybrid catalysts. It was observed that the formation of transition metal complexes inside MCM-41 pores caused a decrease in the pore volume of support. This is the result of formation of complexes inside the Al-MCM-41 cavities. The increase in surface area of catalysts compared to mesoporous materials is because of the increase in crystallinity of samples as proved by the increase in the intensity of d$_{100}$ diffraction peak.

Table 5: Surface area and pore volume data of Al-MCM-41 before and after encapsulation

Sample	Specific surface area, BET (m^2/g)		Pore volume (cm^3/g)	
	Before	After	Before	After
Al-MCM-41(C$_{10}$)	665	702	0.71	0.62
Al-MCM-41(C$_{16}$)	904	947	0.97	0.88
Al-MCM-41(C$_{18}$)	1017	1060	1.09	9.85

All samples obtained from heterogenization process show that the catalysts do not have any significant differences from those of Al-MCM-41, except for the slight decrease in intensity of d$_{100}$ diffraction peak, as shown in Figure 9. This proves that the hexagonal long range ordered structure of support is preserved after modification with a slight decrease in crystallinity and uniformity, as the pore dimension is

wide enough to accommodate the complex molecules (Guan, 2005). Figure 10 shows that there is still increasing trend in the pore diameter of the samples as the length of the templates used was increased. As shown in Table 6, the heterogenization of ligand results in an increase in the unit cell parameter, a_o of catalyst, as observed by the decrease in 2θ value. The increase of size of pore diameter of Al-MCM-41 is because of the steric effect in the presence of bulky organic molecules (Kim and Park, 2000; Kureshy, 2003).
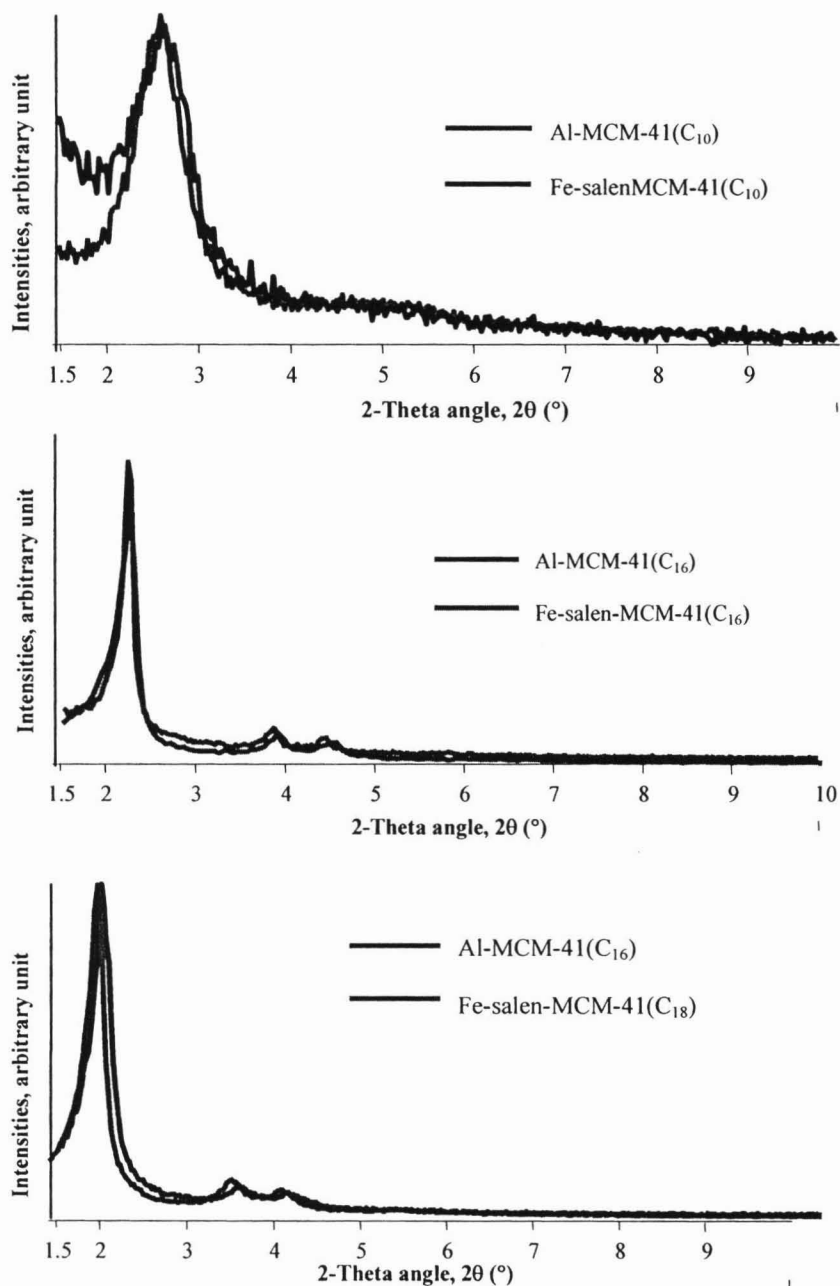
Figure 9: X-ray diffractogram of Al-MCM-41(C_{10}), Al-MCM-41(C_{16}) and Al-MCM-41(C_{18}) samples; before and after immobilization process
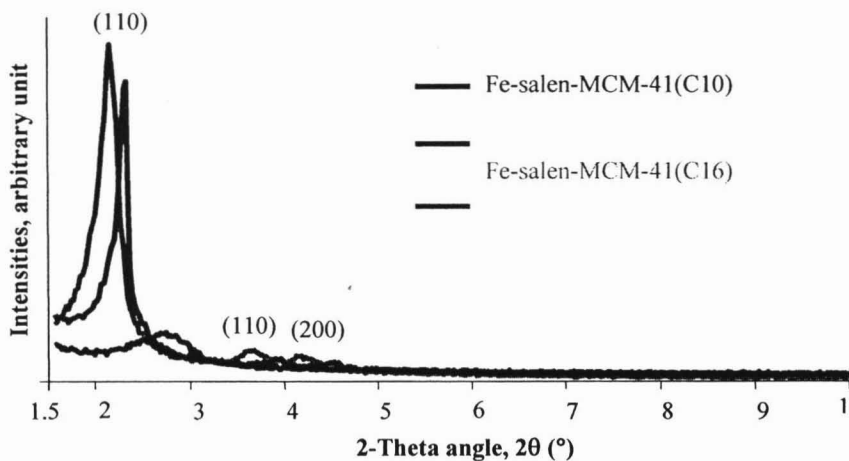
Figure 10: X-ray diffractograms of hybrid catalysts

Table 6: Effect of complexation on support

Sample	FSM(C₁₀)	FSM(C₁₆)	FSM(C₁₈)
Intensity of d_{100} peak (Count)	688	4564	5190
2-Theta angle, 2θ (°)	2.7	2.2	2.1
Hexagonal lattice parameter, d_{100} (nm)	3.2	3.9	4.1
Hexagonal unit cell parameter, a_0 (nm)	3.7	4.5	4.7
Pore diameter, (nm)	2.7	3.5	3.7

UV-Vis spectra of prepared hybrid catalysts are shown in Figure 11. Based on this spectra, it is proven that the encapsulated Fe(salen) shows identical UV-Vis spectrum of neat metal complex, which have two absorption peaks at around 400 and 500 which indicate the charge transfer transition between the metal and ligand (d-π^*) in the –C=N-M group and d-d electronic transition, respectively. This indicates that the geometry and electronic surrounding of both catalytic systems are the same (Kim & Park, 2000).
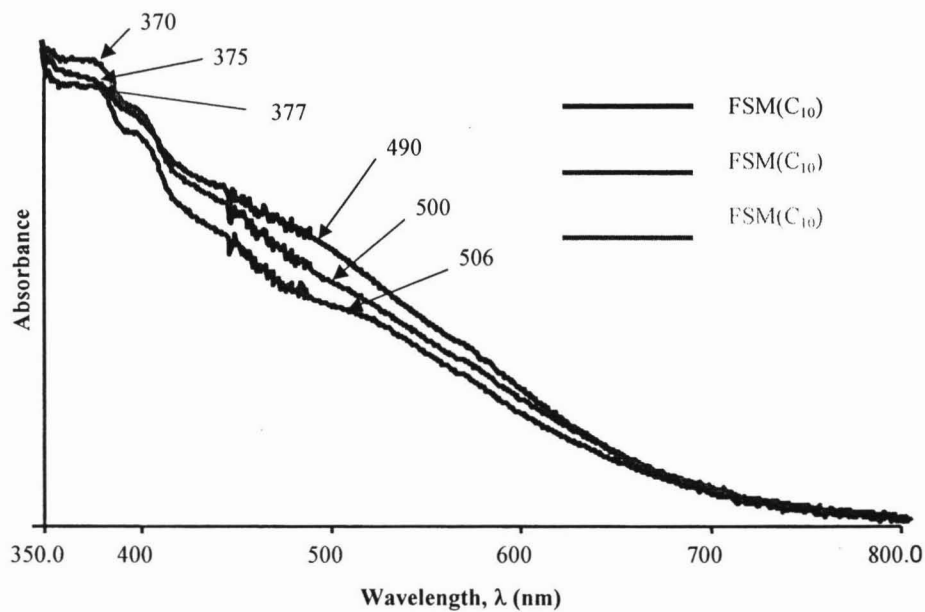

Figure 11: UV-Vis spectra of the synthesized hybrid catalysts

149

The images from FESEM, Figure 12 below show the topography of Fe-salen-MCM-41(C_{10}), Fe-salen-MCM-41(C_{16}) and Fe-salen-MCM-41(C_{18}) which gave a fungus-like look. The particles size range of each catalyst showed in Table 7 below while the percentage of Fe ions present in the catalysts, which was determined by EDX listed in Table 7 for FSM10, FSM16 and FSM 18, respectively.
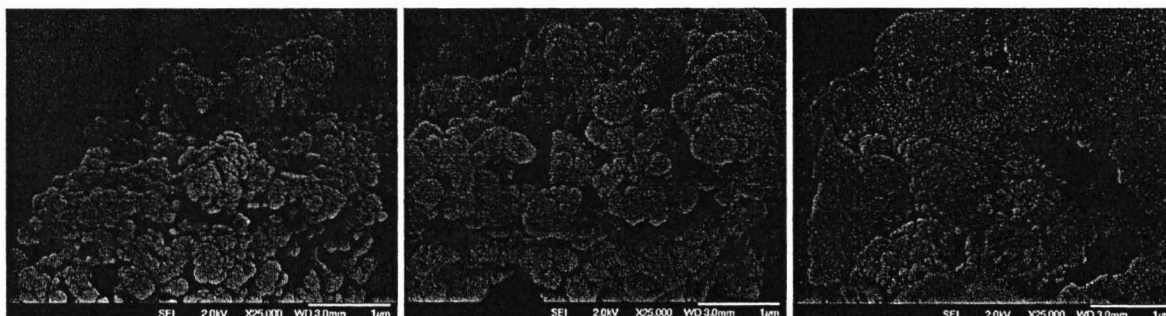
Figure 12: FESEM image of a) Fe-salen-MCM-41(C_{10}), b) Fe-salen-MCM-41(C_{16}) and c) Fe-salen-MCM-41(C_{18})

Table 7: Particles size range of each catalyst

Catalysts	FSM10	FSM16	FSM18
Particles size range (nm)	14.8-29.8	21.6-34.8	19.4-52.6

Table 8: Mass percentage of Fe ions present in the catalysts

Catalysts	FSM10	FSM16	FSM18
Mass of Fe in catalyst (%)	1.32	1.36	1.59

Conclusion

Characterization of the synthesized Al-MCM-41(C_{10}), Al-MCM-41(C_{16}) and Al-MCM-41(C_{18}) using XRD shows that the three supports were successfully synthesized. Upon calcination, the crystallinity of the as-synthesized samples increase, while the pore diameter decrease because of template removal. There is an increasing trend in the pore diameter of the samples as the length of the template used increase. This was established by specific surface area analysis using BET in which the sample synthesized using longer carbon chain template gave higher surface area and pore volume. Salen ligand was successfully synthesized using reaction of salicylaldehyde and ethylenediamine. This was proven by the appearance of the new C=N absorption peak in FTIR spectrum. The complexation process to produce salen complex was successful as observed in shifting of C=N absorption peak to lower wavelength number which shows the metal-ligand interaction. The UV-Vis spectrum of the salen complex shows the existence of two signals assigned to ligand charge band and d-d electronic transition which indicates the successful coordination of ligand to Fe ion center. The d-d transition gives the bright yellow color to the complex. The immobilization of Fe(salen) complex onto three sizes of Al-MCM-41 supports to produce hybrid catalyst via flexible ligand method was successful. The XRD result shows that the supports remain intact after immobilization. FTIR spectra of catalyst show the appearance of new absorption peaks which are absent in spectra of the supports. The UV-Vis spectra of catalyst shows that the geometry and electronic surrounding salen complex remain.

References

Balkus, K. J., & Gabrielov, A. G. (1995). Zeolite Encapsulated Metal Complexes. *Journal of Inclusion Phenomena and Molecular Recognition in Chemistry*. 21: 159-184.

Daud, A. M. (2006). MSc. Thesis Universiti Teknologi Malaysia.

Doménech, A., Formentin, P., García, H. & Sabater, M. J. (2000). Combined Electrochemical and EPR Studies of Manganese Schiff Base Complexes Encapsulated within the Cavities of Zeolite Y. *Eur. J. Inorg. Chem.* 1339-1344.

Flanigen, E. M. (1976). Structural Analysis by Infrared Spectroscopy in Zeolite Chemistry and Catalysis. In: Rabo, J. A. *Zeolite Chemistry and Catalysis*. ACS Monograph. 80-117.

Guan, L.C. (2005). *Mesoporous MCM-48 Synthesized from Rice Husk Ash Silica: Physicochemical Properties and Its Catalytic Activity in Acylation Reaction.* MSc. Thesis. Universiti Teknologi Malaysia.

Grun, M., Unger, K. K., Matsumoto, A., & Tsutsumi, K. (1999). Novel Pathways for the Preparation of Mesoporous MCM-41 Materials: Control of Porosity and Morphology. *Microporous and Mesoporous Materials*. 27: 207-216.

Hu X., Foo M. L., Chuah G. K., & Jaenicke S. (2000). Pore Size Engineering of MCM-41: Selectivity Tuning of Heterogenized $AlCl_3$ for the Synthesis of Linear Alkyl Benzenes. *Journal of Catalyst.* 195: 412-415.

Karandikar, P., Agashe, M., Vijayamohanan, K., & Chanwadkar, A. J. (2004). Cu^{2+}-Perchlorophthalocyanine Immobilized MCM-41: Catalyst for Oxidation of Alkenes. *Applied Catalysis A: General.* 257: 133-143.

Kim, G. J., & Park, D. W. (2000). The Catalytic Activity of New Chiral Salen Complexes Immobilized on MCM-41 in the Asymmetric Hydrolysis of Epoxides to Diols. *Catalysis Today.* 63: 537-547.

Kubota Y., Ikeya H., Sugi Y., Yamada T., & Tatsumi T. (2006). Organic-Inorganic Hybrid Catalysts Based on Ordered Porous Structures for Michael Reaction. *Journal of Molecular Catalysis A:Chemical.* 249: 181-190.

Kureshy, R. I., Khan, N. H., Abdi, S. H. R., Ahmad, I., Singh, S., & Jasra, R. V. (2003). Immobilization of Dicationic Mn(III) Salen in the Interlayers of Montmorillonite Clay for Enantioselective Epoxidation of Nonfunctionalized Alkenes. *Catalysis Letters.* 91(3-4): 207-210.

Ravikovitch, P. I., Wei, D., Chueh, W. T., Haller, G. L., & Neimark, A. V. (2003). Evaluation of Pore Structure Parameters of MCM-41 Catalyst Supports and Catalysts by Means of Nitrogen and Argon Adsorption. *J.Phys.Chem.B.* 101: 3671-3679.

Rino Rakhmata Mukti. (2003). H-Al-MCM-41 in the Benzoylation of Biphenyl for the Formation of Disubstituted 4,4'-Dibenzoylbiphenyl. MSc. Thesis. Universiti Teknologi Malaysia.

Sayari A. (1996). Catalysis by Crystalline Mesoporous Molecular Sieves. *Chem. Mater.* 8: 1840-1852.

Shriver, D. F., & Atkins, P. W. (1999). *Inorganic Chemistry.* London: Oxford University Press.

Wight, A.P., & Davis M. E. (2002). Design and Preparation of Organic-Inorganic Hybrid Catalysts. *Chem. Rev.* 102: 3589-3614.